RSC Advances

ROYAL SOCIETY OF CHEMISTRY

PAPER

View Article Online
View Journal | View Issue

Check for updates

Cite this: *RSC Adv.*, 2021, **11**, 37677

# A novel $Ce_{0.8}Fe_{0.1}Zr_{0.1}O_2$ solid solution with high catalytic activity for hydrogen storage in $MgH_2$

Ying Cheng,[a] Shuhua Zhou,[b] Biqing Shi,[a] Bing Dong,[a] Xianbin Ji,[a] Siqi Li[a] and Wei Zhang *[b]

Received 16th September 2021
Accepted 3rd November 2021

DOI: 10.1039/d1ra06951a

rsc.li/rsc-advances

The effect of the solid solution $Ce_{0.8}Fe_{0.1}Zr_{0.1}O_2$, successfully prepared by a hydrothermal synthesis method, on the hydrogen sorption properties of $MgH_2$ is systemically investigated. The $Ce_{0.8}Fe_{0.1}Zr_{0.1}O_2$-modified $MgH_2$ composite exhibits remarkable hydrogen kinetics properties and thermodynamics behavior compared to those of as-milled $MgH_2$, with a reduction in the initial desorption temperature of approximately 82 K. With respect to the hydrogen kinetics, the $Ce_{0.8}Fe_{0.1}Zr_{0.1}O_2$-added sample could uptake approximately 5.3 wt% $H_2$ at 473 K in 2500 s, whereas only 1.5 wt% hydrogen could be absorbed by pristine $MgH_2$ in the same conditions. Furthermore, about 4.5 wt% of hydrogen could be desorbed by $Ce_{0.8}Fe_{0.1}Zr_{0.1}O_2$-doped $MgH_2$ composite at 623 K, which was 2 wt% higher than the as-milled $MgH_2$ sample over the same period of time. The decomposition apparent activation energy for $MgH_2$–$Ce_{0.8}Fe_{0.1}Zr_{0.1}O_2$ is reduced to 84.3 kJ $mol^{-1}$, which is about 77 kJ $mol^{-1}$ lower than that of pristine $MgH_2$. It is believed that the notable improvement in the hydrogen sorption kinetics is due to the *in situ*-formed active species of $CeH_{2.51}$ and MgO as well as the abundant oxygen vacancies, which play a vital role in catalyzing the hydrogen sorption performance of $MgH_2$.

## 1. Introduction

Hydrogen, as a green fuel, is seen as one of the most promising energy carriers due to its high energy density, cost-effectiveness, and non-pollution, which could also efficiently solve the major issues in regard to fossil fuels: urban air pollution and climate change impact.[1,2] To make full use of hydrogen energy sources and realize hydrogen economy, many factors, including production, distribution, transportation, and storage need to be considered. The key to the widespread utilization of hydrogen is to develop safe and efficient storage materials for hydrogen. It is generally accepted that solid-state hydrogen storage materials act like a sponge with the ability to absorb and release hydrogen, which make them propitious candidates for hydrogen storage. Among the solid-state hydrogen storage materials, magnesium has received much attention owing to its high hydrogen capacity, abundant availability, and low cost. However, to make $MgH_2$ a benign and viable hydrogen storage material, two critical barriers need to be overcome. It is well known that $MgH_2$ possesses superior stability and relatively high temperatures are needed to decompose the Mg–H bond to release $H_2$.

Numerous methods have been optimized to overcome the disadvantages of $MgH_2$ by ball-milling, nano-structuring, alloying, catalyst doping, *etc.* Among them, ball-milling various metal catalysts with $MgH_2$ is considered an efficient way to significantly improve the hydrogen storage properties of $MgH_2$. One of the well-known ergastic additives is the rare earth material ceria (Ce). A large number of experiments have been launched to study the catalytic effect of Ce-based materials. Ismail *et al.*[3] reported that doping with $CeCl_3$ could significantly reduce the initial decomposition temperature and enhance the sorption kinetics of $MgH_2$. Some research showed that the peak temperature and the decomposition apparent activation energy for the hydrogen desorption of Mg–20Ni–$CeO_2$ decreased to 318.9 °C and 72.7 kJ $mol^{-1}$ due to the presence of $CeO_2$.[4] Leng *et al.*[5] systemically investigated the influence of Ce on $TiFe_{0.9}$-$Mn_{0.1}$ alloy and found that the addition of Ce significantly enhanced the hydrogen storage properties of $TiFe_{0.9}Mn_{0.1}$ alloy on account of its high dispersion on the $TiFe_{0.9}Mn_{0.1}$ matrix.

Fe has also been widely proved to be an effective catalyst that can promote remarkable improvement of the hydrogen absorption and desorption performances of $MgH_2$.[6] Chen *et al.*[7] prepared nanosheet Fe through a wet-chemical ball milling method which contributes to the enhancement of the hydrogen storage properties of $MgH_2$. Wang and Yan *et al.*[8] have shown the improved kinetics results of $MgH_2$ catalyzed by FeB/CNTs; the composites could absorb about 6.2 wt% of hydrogen at 150 °C. Song *et al.*[9] prepared $MgH_2$ catalyzed by 10 wt% $Fe_2O_3$ through a mechanical milling method. They reported that 10 wt% $Fe_2O_3$ shows far better hydrogen/dehydrogen storage behaviors compared to pristine $MgH_2$.

[a]Department of Environmental Engineering, Hebei University of Environmental Engineering, Qinhuangdao, 066102, PR China

[b]Hebei Key Laboratory of Applied Chemistry, School of Environmental and Chemical Engineering, Yanshan University, Qinhuangdao 066004, PR China. E-mail: zhangweihh@ysu.edu.cn; Tel: +86-010-8387744

Furthermore, recent studies have demonstrated that oxygen vacancies ($O_{vac}$) are greatly important active sites for hydrogen storage which can capture $H_2$ molecules and help the diffusion of H atoms during the hydrogen absorption/desorption processes.[10] The enhancement of hydrogen dynamics and thermodynamics properties is mainly ascribed to the abundant oxygen vacancies, as confirmed by Zhou *et al.*[11] An abundance of oxygen vacancies can be achieved by the addition of Zr into $CeO_2$.[12,13] Moreover, extensive research has revealed that the density of oxygen vacancies on transition doped Ce–Zr oxides is far better than on single Ce–Zr oxides;[14,15] $O_{vac}$ defects can be produced on the $CeO_2$ surface by $Ce^{3+}$–$Ce^{4+}$ transfer owing to the transition metal dopant.

Inspired by these studies, a Ce–Fe–Zr oxide solid solution catalyst with high activity and $O_{vac}$ defects was designed and the influence of the Ce–Fe–Zr solid solution on the hydrogen storage properties of $MgH_2$ was systemically investigated. Moreover, the catalytic mechanism of the synthesized Ce–Fe–Zr solid solution in $MgH_2$ is explained, which will provide novel strategies for the design of multiple catalysts and enrich the hydrogen storage field.

## 2. Experimental section

### 2.1 Synthesis of $Ce_{0.8}Fe_{0.1}Zr_{0.1}O_2$ catalyst

$Ce(NO_3)_3 \cdot 6H_2O$ (99.9%), $ZrOCl_2$ (99.9%) and $Fe(NO_3)_3 \cdot 6H_2O$ (99.9%) were purchased from Aladdin Chemical Reagent Co. Ltd and used as reactants without any purification. The above reactants in a mass ratio of 8 : 1 : 1 were dissolved in a solvent composed of CTAB with $NH_3 \cdot H_2O$ added dropwise into the mixed solution to adjust the pH to 9–11. The mixture was stirred in the reactor for 1–2 hours and then stood at room temperature for 12 hours. After standing, the solution was filtered and washed several times with deionized water, then put into an oven at 60 °C to dry for 12 h. After drying, the sample was calcined in a muffle furnace and raised to the target temperature of 550 °C at a rate of 1 °C $min^{-1}$. After holding at the target temperature for a period, the solid solution of cerium zirconium was obtained.

### 2.2 Synthesis of $MgH_2$–$Ce_{0.8}Fe_{0.1}Zr_{0.1}O_2$ composites

$MgH_2$ was prepared from commercial Mg powder (98%) through hydrogen combustion. The Mg powder was purchased from Aladdin Chemical Reagent Co. Ltd and hydrogenated at 400 °C at 4 MPa for 10 h. Pure $MgH_2$ was successfully obtained by repeating the above procedure five times.

The doped $MgH_2$–$Ce_{0.8}Fe_{0.1}Zr_{0.1}O_2$ sample was fabricated through a mechanical ball-milling method by milling $MgH_2$ and $Ce_{0.8}Fe_{0.1}Zr_{0.1}O_2$ in a mass ratio of 5 : 1. An increased milling temperature was inhibited by controlling the mill direction, starting in one direction for 15 min, switching to the opposite direction for 15 min and then pausing for 10 min. The ball-to-sample weight ratio was 20 : 1. To prevent the sample from contacting oxygen and vapor, the operation was conducted in an Ar-filled glove box.

### 2.3 Characterization

X-ray diffraction (XRD) was conducted on a SmartLab high resolution X-ray diffractometer (Rigaku) with Cu K$\alpha$ radiation at 40 kV and 40 mA. The scanning speed was 4° $min^{-1}$ in the range of 10° to 80°. Scanning electron microscopy (SEM) was employed to observe the micro-structure and morphology of the formed sample. The element distribution and active oxygen species on the surface of the catalyst were determined by X-ray photoelectron spectroscopy (XPS).

The measurements of the initial desorption temperature and hydrogen absorption/desorption kinetics were performed on a Sieverts-type pressure-composition-temperature (PCT) apparatus (GRINM Co., China). During the initial desorption temperature test, the sample was heated from room temperature to 1000 K at 0.01 MPa with a heating rate of 10 K $min^{-1}$ in a vacuum chamber. For the hydrogen absorption kinetics tests, the sample was heated to 473 K and 523 K under 3.0 MPa of pressure, while for the hydrogen desorption kinetics tests, the sample was heated to 598 K and 623 K under a pressure of 0.001 MPa. The thermal behaviors of the as-milled $MgH_2$ and $Ce_{0.8}Fe_{0.1}Zr_{0.1}O_2$-catalyzed $MgH_2$ were examined by differential scanning calorimetry (Mettler Toledo, TGA/DSC 1). All the samples were heated under an Ar atmosphere from room temperature to 500 °C at heating rates of 5 K $min^{-1}$, 10 K $min^{-1}$, 15 K $min^{-1}$, and 20 K $min^{-1}$.

## 3. Results and discussion

### 3.1 Characteristics of the prepared $Ce_{0.8}Fe_{0.1}Zr_{0.1}O_2$

The XRD pattern of the synthesized $Ce_{0.8}Fe_{0.1}Zr_{0.1}O_2$ in Fig. 1 obviously shows strong peaks at $2\theta = 28.86°$, 33.52°, 47.78°, 56.66°, 59.63°, 70.35°, 77.56°, and 78.19° which correspond well to the standard card (PDF# 34-0394). All the strong peaks are shifted to the left compared to the standard card (PDF# 34-0394), indicating the successful synthesis of the solid solution $Ce_{0.8}Fe_{0.1}Zr_{0.1}O_2$ catalyst.

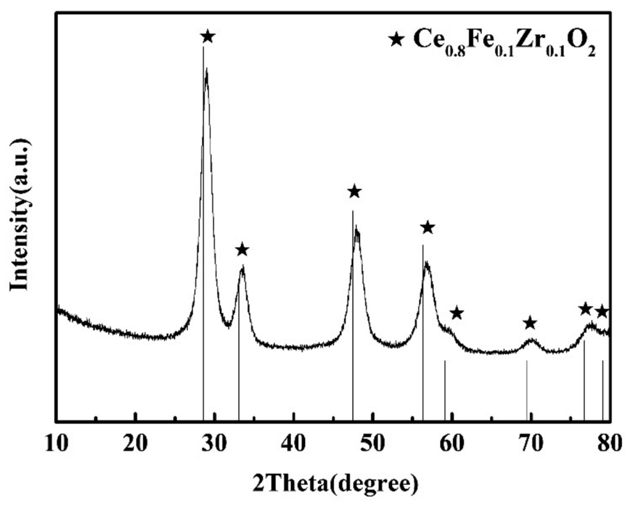


Fig. 1 XRD pattern of $Ce_{0.8}Fe_{0.1}Zr_{0.1}O_2$ catalyst.

 

### 3.2 TPD curves of $MgH_2$–$Ce_{0.8}Fe_{0.1}Zr_{0.1}O_2$ and $MgH_2$ samples

Fig. 2 depicts the temperature programmed desorption (TPD) patterns for the hydrogen desorption process of ball-milled $MgH_2$ and $Ce_{0.8}Fe_{0.1}Zr_{0.1}O_2$-catalyzed $MgH_2$ materials. The ball-milled pristine $MgH_2$ begins to release hydrogen at about 643 K, with a maximum hydrogen capacity of about 6.5 wt% of hydrogen reached by 800 K. Moreover, $Ce_{0.8}Fe_{0.1}Zr_{0.1}O_2$ contributes to the hydrogen desorption of $MgH_2$ in a relatively lower temperature range than that of pure $MgH_2$. An obvious feature seen in Fig. 2 is that $Ce_{0.8}Fe_{0.1}Zr_{0.1}O_2$-catalyzed $MgH_2$ starts to release hydrogen at a lower temperature, approximately 561 K, achieving a full hydrogen capacity of about 5.5 wt% $H_2$ at 690 K. Furthermore, the modified sample completed dehydrogenation at 710 K. In contrast, the saturation of the desorption process for pure $MgH_2$ is at 830 K. According to the TPD curves, the desorption rate and temperature determined for $Ce_{0.8}Fe_{0.1}Zr_{0.1}O_2$-catalyzed $MgH_2$ are superior to those of $MgH_2$ without the catalyst. The onset temperature reduction (82 K) on the doped sample signifies that $Ce_{0.8}Fe_{0.1}Zr_{0.1}O_2$ is a promising catalyst in the $MgH_2$ system which helps lower the desorption temperature and rate.

### 3.3 Sorption kinetics of $MgH_2$–$Ce_{0.8}Fe_{0.1}Zr_{0.1}O_2$ and $MgH_2$ samples

Further investigation of the catalytic activity of $Ce_{0.8}Fe_{0.1}Zr_{0.1}O_2$ on the hydrogen desorption properties of $MgH_2$ was performed by hydrogen sorption release. Fig. 3 exhibits the hydrogen desorption properties for the milled $MgH_2$ and the modified sample at 598 K and 623 K. It is obvious that the ball-milled $MgH_2$ shows sluggish desorption kinetic properties compared to those with catalyst addition at the investigated temperature. Almost no hydrogen is released by $MgH_2$ at the temperature of 598 K. At this temperature, the $Ce_{0.8}Fe_{0.1}Zr_{0.1}O_2$-doped $MgH_2$ yields a significant increase to 2.5 wt% hydrogen at 598 K within 2000 s. When the temperature shows a sharp shift to 623 K, both the hydrogen desorption properties and desorption rate are

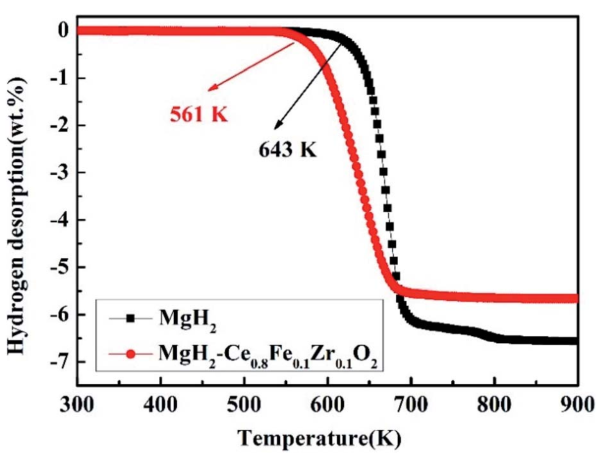


Fig. 2 TPD curves of ball-milled $MgH_2$ and $Ce_{0.8}Fe_{0.1}Zr_{0.1}O_2$-catalyzed $MgH_2$ at the heating rate of 10 K $min^{-1}$.

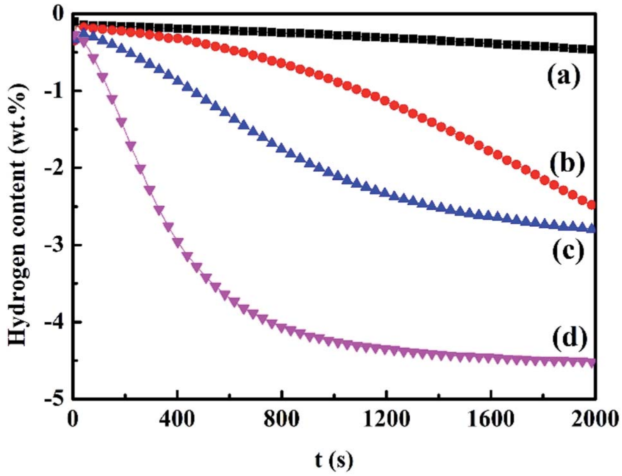


Fig. 3 Desorption kinetics curves of ball-milled $MgH_2$ at 598 K (a) and 623 K (b) and $Ce_{0.8}Fe_{0.1}Zr_{0.1}O_2$ catalyzed $MgH_2$ at 598 K (c) and 623 K (d).

highly improved. The $Ce_{0.8}Fe_{0.1}Zr_{0.1}O_2$-added sample results in the liberation of approximately 4.5 wt% hydrogen at 623 K after 2000 s of dehydrogenation, whereas the as-milled $MgH_2$ sample desorbs less than 2.5 wt% hydrogen over the same period. It is evident that $Ce_{0.8}Fe_{0.1}Zr_{0.1}O_2$ plays a significant catalytic role in enhancing the desorption behavior of $MgH_2$.

The excellent hydrogen release kinetics of $MgH_2$ are related to the energy barrier of the desorption process on $MgH_2$ and the apparent energy ($E_a$) is a key parameter that reflects the improved desorption kinetics. To determine the $E_a$ for the desorption stage, the Kissinger method was used. The equation is as follows:

$$\frac{d\left[\ln\left(\alpha/T_m{}^2\right)\right]}{d(1/T_m)} = \frac{-E_a}{R} \tag{1}$$

where $\alpha$ is the different rise rates (K $min^{-1}$), $T_m$ is the peak temperature for the different desorption rates (K), and $R$ is the gas constant of 8.314 J (mol K)$^{-1}$. Fig. 4 displays the DSC curves of $MgH_2$ and $Ce_{0.8}Fe_{0.1}Zr_{0.1}O_2$-catalyzed $MgH_2$ composite at various heating rates. It can be noted that the slopes for the undoped and doped samples are −19.39 and −10.14, respectively, and the value of the activation energy for the milled $MgH_2$ is estimated to be 161.2 kJ $mol^{-1}$, while the value of the $Ce_{0.8}Fe_{0.1}Zr_{0.1}O_2$-doped sample is 84.3 kJ $mol^{-1}$, much lower than that of the milled $MgH_2$. In addition, it should be mentioned that this $E_a$ value is lower than or close to those of other $MgH_2$-catalyst composites reported recently, including *o*-$Nb_2O_5$ (101.0 ± 5 kJ $mol^{-1}$), $BaFe_{12}O_{19}$ (115 kJ $mol^{-1}$), $MoO_3$ (114.7 kJ $mol^{-1}$), FeCoNi@GS (85.14 kJ $mol^{-1}$), $MgNiO_2$ (108.0 kJ $mol^{-1}$), Ti containing phase(s) (110.9 kJ $mol^{-1}$) and $LaFeO_3$ (107.0 kJ $mol^{-1}$).[16–22] The value of $E_a$ obtained from the Kissinger equation shows that the kinetics barrier during the desorption process decreased in the presence of $Ce_{0.8}Fe_{0.1}Zr_{0.1}O_2$, thus promoting the hydrogen desorption properties of $MgH_2$.

To further clarify the effect of the synthesized $Ce_{0.8}Fe_{0.1}Zr_{0.1}O_2$ on the hydrogen sorption performance of pristine $MgH_2$, the

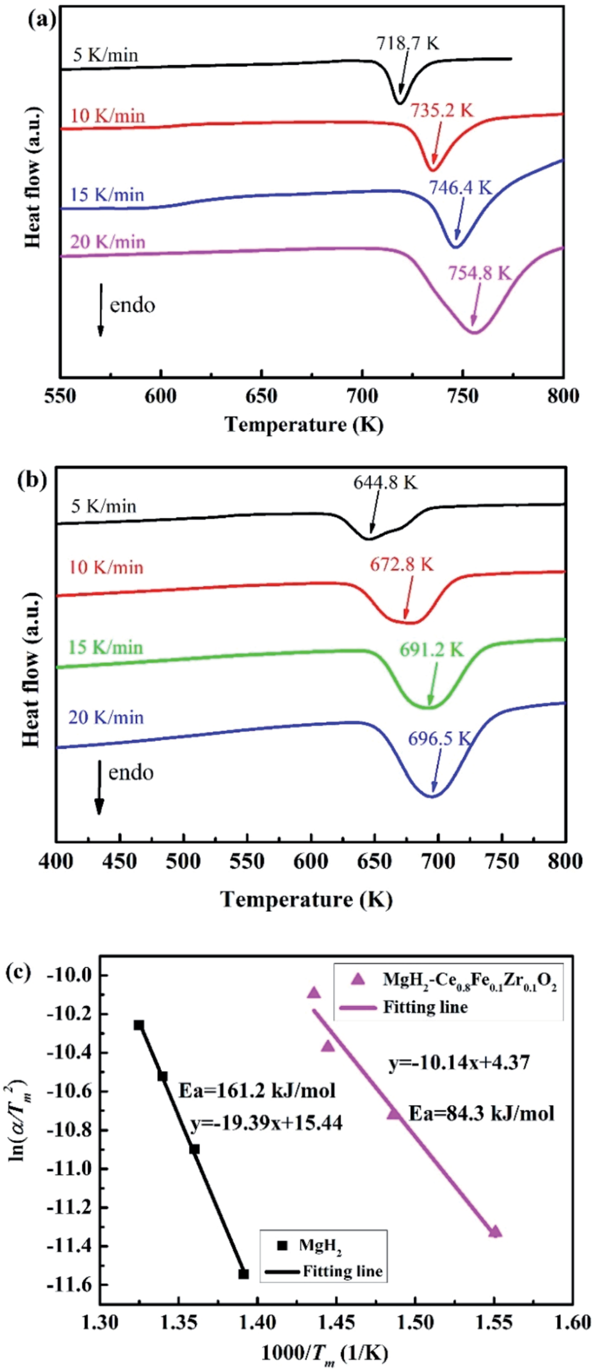


Fig. 4 DSC curves of $MgH_2$ (a) and $Ce_{0.8}Fe_{0.1}Zr_{0.1}O_2$-catalyzed $MgH_2$ (b) at different heating rates; (c) Kissinger's plots for milled $MgH_2$ and $MgH_2$–$Ce_{0.8}Fe_{0.1}Zr_{0.1}O_2$ composite.

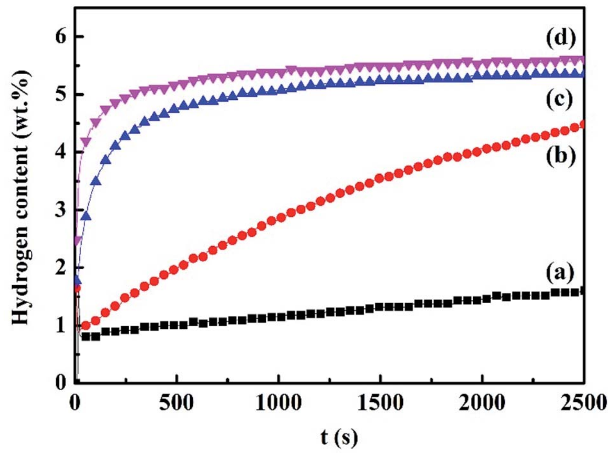


Fig. 5 Absorption kinetics curves of ball-milled samples at different temperatures under 3.0 MPa $H_2$:$MgH_2$ at 473 K (a) and 523 K (b) and $Ce_{0.8}Fe_{0.1}Zr_{0.1}O_2$-catalyzed $MgH_2$ at 473 K (c) and 523 K (d).

isothermal hydrogen absorption was systematically investigated. Fig. 5 collates the findings of the isothermal rehydrogenation kinetics at 473 K and 523 K in the presence of 3.0 MPa hydrogen pressure which demonstrate that the sample of $Ce_{0.8}Fe_{0.1}Zr_{0.1}O_2$ takes in hydrogen faster than pure $MgH_2$ and the $MgH_2$–$Ce_{0.8}Fe_{0.1}Zr_{0.1}O_2$ sample has the superior hydrogen absorption kinetics rate. At 473 K, only 1.5 wt% of hydrogen could be absorbed by pristine $MgH_2$ in 2500 s. For the $Ce_{0.8}Fe_{0.1}Zr_{0.1}O_2$-modified $MgH_2$ sample, the hydrogen absorption capacity is about three times higher than that of pure $MgH_2$, with 5.3 wt% of hydrogen adsorbed. Raising the temperature to 598 K leads to a significant increase in hydrogen capacity as well as in the hydrogen rate compared to those presented by the other sample at the identical temperature. The ball-milled $MgH_2$ presents a slight increase when the temperature rises from 473 K to 523 K, absorbing about 4.4 wt% hydrogen after 2500 s at 523 K. The hydrogen capacity for the modified $Ce_{0.8}Fe_{0.1}Zr_{0.1}O_2$ sample achieves 5.6 wt% hydrogen in the same conditions. The results signify that $Ce_{0.8}Fe_{0.1}Zr_{0.1}O_2$ is a striking catalyst that endows the $MgH_2$–$Ce_{0.8}Fe_{0.1}Zr_{0.1}O_2$ sample with excellent hydrogen absorption behavior. Many researchers have reported a similar phenomenon where increased temperature exhibits a promising effect on the hydrogen storage capacity and hydrogen storage rate of solid-state hydrogen storage materials.[23]

In order to verify the cause of the improvement of the hydrogen absorption kinetics for $MgH_2$ attributed to the addition of $Ce_{0.8}Fe_{0.1}Zr_{0.1}O_2$, the hydrogenation mechanism was investigated by comparing the hydrogen absorption rate curves with the rate equations for $MgH_2$–$Ce_{0.8}Fe_{0.1}Zr_{0.1}O_2$ and $MgH_2$ composites. The Avrami–Erofeev equation (eqn (2)) is usually employed to fit the hydrogenation absorption process and gives strong insight into the nucleation and growth processes.

$$\alpha = 1 - \exp(-kt^m) \tag{2}$$

Here, $\alpha$ is the reacted fraction, $k$ is the rate constant, and $m$ is the order of the reaction. Based on the obtained results, it is evident that there exists a distinct difference between the hydrogen sorption kinetics and the fitting curves result for $MgH_2$. The same phenomenon does not appear in the $Ce_{0.8}Fe_{0.1}Zr_{0.1}O_2$-catalyzed $MgH_2$. It is obvious that for the $Ce_{0.8}Fe_{0.1}Zr_{0.1}O_2$-catalyzed $MgH_2$ composites, the correlation and fitting degree of both curves agree very well. The fitting lines in Fig. 6 depict that the reaction mechanism of $MgH_2$ catalyzed by the $Ce_{0.8}Fe_{0.1}Zr_{0.1}O_2$ composite is subject to nucleation and growth processes. The value of $m$ gives a specific explanation of the rate-controlling step for the hydrogenation diffusion process. It is reported that an $m$ value approaching 0.620 belongs to a one-dimensional diffusion process, whereas a value approximating 1.070 could be ascribed to a three-dimensional diffusional process; a one-dimensional diffusion process is beneficial to hydrogen adsorption.[24] According to the fitted curves, the $m$ value for as-milled $MgH_2$ is equal to 0.91, which is close to 1.070, indicating that the hydrogen sorption process for pure $MgH_2$ is a three-dimensional diffusion process. For the $MgH_2$ catalyzed by $Ce_{0.8}Fe_{0.1}Zr_{0.1}O_2$, the value of $m$ (0.36) approaches 0.620, which indicates one-dimensional diffusion. Therefore, the rate-controlling step for the hydrogenation process changes from a three-dimensional diffusion process to a one-dimensional diffusion process due to the addition of $Ce_{0.8}Fe_{0.1}Zr_{0.1}O_2$.

### 3.4 XRD analysis

To further investigate the reaction mechanism of the improved hydrogenation/dehydrogenation kinetics and thermodynamics of $Ce_{0.8}Fe_{0.1}Zr_{0.1}O_2$-catalyzed $MgH_2$, XRD was employed to clarify the phase components of $MgH_2$–$Ce_{0.8}Fe_{0.1}Zr_{0.1}O_2$ composites at different stages; the XRD patterns are presented in Fig. 7. At the ball-milled stage in Fig. 7a, the dominant diffraction peak is indexed to $MgH_2$ and some new peaks relating to $CeH_{2.51}$ could be detected. Additionally, a diffraction peak at $2\theta = 42.5°$ ascribed to MgO could be found. The appearance of MgO may be due to slight oxygen contamination during XRD. The newly formed phase gives an indication that there has been a chemical reaction between $Ce_{0.8}Fe_{0.1}Zr_{0.1}O_2$ and $MgH_2$ during the ball-milling process. After the composites were hydrogenated at 3.0 MPa (Fig. 7b), all the diffraction peaks become sharper and narrower compared to those of the ball-milled stage and the diffraction peaks for $MgH_2$ and $CeH_{2.51}$ remain. In the XRD pattern of the dehydrogenated sample at 623 K (Fig. 7c), the characteristic diffraction peaks for $MgH_2$ vanish, while those for Mg are obvious, indicating that $MgH_2$

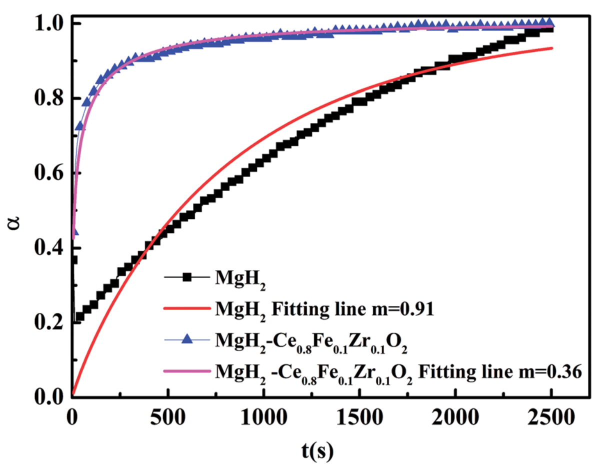


Fig. 6 Fitted hydrogenation kinetic curves of $MgH_2$ and $Ce_{0.8}Fe_{0.1}Zr_{0.1}O_2$-catalyzed $MgH_2$ composite at 523 K under the pressure of 3 MPa.

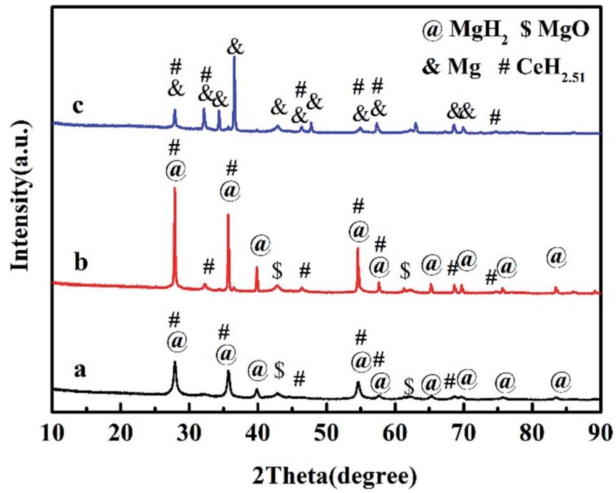


Fig. 7 XRD patterns of $Ce_{0.8}Fe_{0.1}Zr_{0.1}O_2$-catalyzed $MgH_2$ at different stages: (a) after ball-milling, (b) hydrogenation at 3.0 MPa and (c) dehydrogenation at 623 K.

has been largely transformed to Mg during the dehydrogenation process. Fe and Zr cannot be detected in the XRD patterns, due to the small amounts or the formation of solid solution, and the obtained results correspond well to the XRD analysis. It is obvious that the diffraction peaks for $CeH_{2.51}$ and MgO remain present through the whole hydrogenation/dehydrogenation process. It has been confirmed by numerous studies that $CeH_{2.51}$ is beneficial to the enhancement of $MgH_2$ hydrogen uptake and release.[25]

### 3.5 XPS analysis

To explain the reason for the improvement of the hydrogen performance by $Ce_{0.8}Fe_{0.1}Zr_{0.1}O_2$-modified $MgH_2$, the chemical states of key elements which play vital roles in the enhancement by $Ce_{0.8}Fe_{0.1}Zr_{0.1}O_2$ are investigated. The Ce 3d and O 1s spectra for $Ce_{0.8}Fe_{0.1}Zr_{0.1}O_2$ are presented with that of pure $CeO_2$ as a comparison. The O 1s spectrum (Fig. 8A) can be divided into three main peaks: the one centered at 529.5 eV, which is related to lattice oxygen $O_\alpha(O^{2-})$, and two others centered at 530.4 and 532.8 eV, which are ascribed to surface chemically adsorbed oxygen $O_\beta(O^-, O_2^-)$.[26] It is obvious that the amount of lattice oxygen $O_\alpha$ on the surface of $Ce_{0.8}Fe_{0.1}Zr_{0.1}O_2$ is higher than that in pure $CeO_2$, indicating that more oxygen vacancies exist in the Fe and Zr doped $CeO_2$.

According to Fig. 8B, the complex spectrum of Ce 3d can be decomposed into eight peaks, labeled as V (882.4 eV), V′ (885.0 eV), V″ (889.2 eV), V‴ (898.1 eV), U (900.9 eV), U′ (903.3 eV), U″ (907.6 eV), and U‴ (916.7 eV). The split peaks labeled V, V″, V‴, U, U″, and U‴ are ascribed to $Ce^{4+}$ species, while the peaks located at V′ and U′ correspond to $Ce^{3+}$ species.[27] The primary chemical valence state on the surface of the sample is $Ce^{3+}$. It can be clearly seen in Fig. 8B that the surface $Ce^{3+}$ amount is higher on $Ce_{0.8}Fe_{0.1}Zr_{0.1}O_2$ than on pure $CeO_2$. Huang[28] and Weng *et al.*[29] confirmed that the improved catalytic activity could be due to the formation of more $Ce^{3+}$ accompanied by

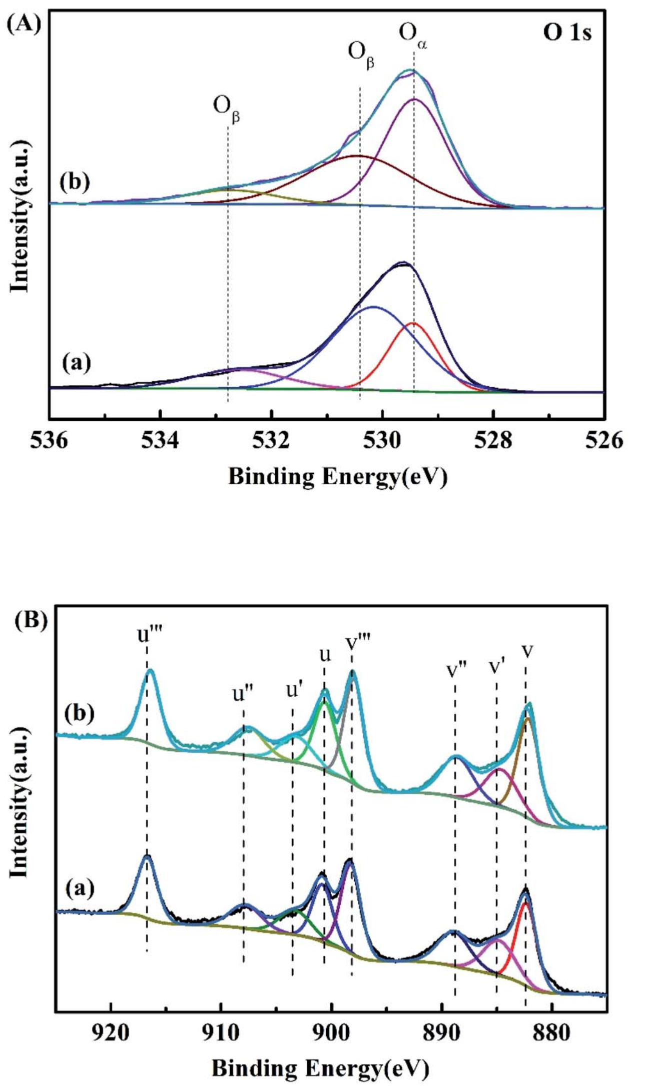


Fig. 8 (A) O 1s XPS spectra of (a) $CeO_2$ and (b) $Ce_{0.8}Fe_{0.1}Zr_{0.1}O_2$; (B) Ce 3d XPS spectra of (a) $CeO_2$ and (b) $Ce_{0.8}Fe_{0.1}Zr_{0.1}O_2$.

oxygen defects. According to the obtained results of the XPS analysis, the Fe and Zr doped $CeO_2$ possesses more oxygen vacancies and $Ce^{3+}$ on the $Ce_{0.8}Fe_{0.1}Zr_{0.1}O_2$ surface.

Based on the XRD and XPS analyses, the catalytic mechanism of $Ce_{0.8}Fe_{0.1}Zr_{0.1}O_2$ that improves the hydrogenation/dehydrogenation properties of $MgH_2$ can be summarized. The generation of $CeH_{2.51}$ and MgO derived from the reaction between $Ce_{0.8}Fe_{0.1}Zr_{0.1}O_2$ and $MgH_2$ may play a vital role in altering the hydrogenation/dehydrogenation behaviors of $MgH_2$. It has been reported by numerous researchers that the *in situ*-formed light rare earth hydride $CeH_{2.51}$ could serve as the real catalyst promoting the hydrogenation/dehydrogenation procedures.[30,31] The light rare earth hydrides generate the activation of the surface of $MgH_2$ and lead to more nucleation sites on the substrate of $MgH_2$, also providing H diffusion channels and easily facilitating the hydrogen absorption and desorption processes.[32] In addition, the produced MgO also brings a positive catalytic effect for the improvement of $MgH_2$. Ismail *et al.*[33] showed that MgO could work with Fe, Mg–Cu alloy as an active species to catalyze the hydrogen storage properties of $MgH_2$ in $CuFe_2O_4$-doped $MgH_2$ composite. MgO also played a crucial role in improving the sorption performance of the $MgH_2$–$MgFe_2O_4$ system through the synergetic catalytic effect.[34] Also, its high electronegativity promotes the improvement of the kinetics of magnesium-based hydrides.[35] Furthermore, the addition of Fe and Zr promotes more oxygen vacancies and $Ce^{3+}$ on the surface of $Ce_{0.8}Fe_{0.1}Zr_{0.1}O_2$ and multi-valence catalysts and abundant oxygen vacancies have shown great potential in enhancing the de/hydrogenation kinetics of $MgH_2$.[11,36] Therefore, the great improvement in the hydrogenation kinetics is ascribed to the *in situ*-formed active species $CeH_{2.51}$ and MgO and the abundant oxygen vacancy defects, which may be the major factors boosting the hydrogen sorption performance of $MgH_2$.

## 4. Conclusions

The solid solution $Ce_{0.8}Fe_{0.1}Zr_{0.1}O_2$ was successfully prepared by hydrothermal synthesis method and exhibited surprisingly high catalytic activity, leading to the $MgH_2$–$Ce_{0.8}Fe_{0.1}Zr_{0.1}O_2$ composite reflecting excellent hydrogen sorption kinetics. The $Ce_{0.8}Fe_{0.1}Zr_{0.1}O_2$-doped $MgH_2$ presented striking hydrogen storage properties as it starts to liberate $H_2$ at 561 K in the dehydrogenation process, 82 K lower than the pristine $MgH_2$. With respect to hydrogen adsorption, the $Ce_{0.8}Fe_{0.1}Zr_{0.1}O_2$-added sample could uptake approximately 5.3 wt% $H_2$ at 473 K, while only 1.5 wt% hydrogen could be absorbed by pristine $MgH_2$ in the same conditions. The dehydrogenation properties of $MgH_2$ are also improved, with a desorption amount of 4.5 wt% hydrogen at 623 K, where the as-milled $MgH_2$ sample desorbs less than 2.5 wt% hydrogen over the same period of time. The Kissinger plot shows that the apparent activation energy for $MgH_2$ is reduced from 161.2 kJ mol$^{-1}$ to 84.3 kJ mol$^{-1}$ due to the presence of the solid solution $Ce_{0.8}Fe_{0.1}Zr_{0.1}O_2$-modified sample. It is believed that the great improvement in hydrogen sorption kinetics is due to the *in situ*-formed active species of $CeH_{2.51}$ and MgO and the abundant oxygen vacancies, which play vital roles in boosting the hydrogen sorption performance of $MgH_2$.

## Conflicts of interest

There are no conflicts to declare.

## Acknowledgements

This work was funded by Natural Science Foundation of Hebei Province of China (E2019415036; B2021415002); Science and Technology Project of Hebei Education Department (BJ2020043; QN2020142); Hebei University of Environmental Engineering (Top-notch Talents Cultivation Program for Young Science and Technology 2020ZRBJ01); Doctoral Foundation of Hebei University of Environmental Engineering (201805).

 

## Notes and references

1 Z. Shao, Y. Li, C. Liu, W. Ai, S.-P. Luo and Q. Liu, *Nat. Commun.*, 2020, **11**, 591.
2 D. J. Han, S. Kim and E. S. Cho, *J. Mater. Chem. A*, 2021, **9**, 9875–9881.
3 M. Ismail, N. S. Mustafa, N. Juahir and F. A. H. Yap, *Mater. Chem. Phys.*, 2016, **170**, 77–82.
4 P. Liu, J. J. Lian, H. P. Chen, X. J. Liu, Y. L. Chen, T. H. Zhang, H. Yu, G. J. Lu and S. X. Zhou, *Chem. Eng. J.*, 2020, **385**, 9.
5 H. Leng, Z. Yu, J. Yin, Q. Li, Z. Wu and K.-C. Chou, *Int. J. Hydrogen Energy*, 2017, **42**, 23731–23736.
6 N. A. Abdul Majid, J. Watanabe and M. Notomi, *Int. J. Hydrogen Energy*, 2021, **46**, 4181–4187.
7 L. Zhang, L. Ji, Z. Yao, N. Yan, Z. Sun, X. Yang, X. Zhu, S. Hu and L. Chen, *Int. J. Hydrogen Energy*, 2019, **44**, 21955–21964.
8 S. Gao, X. Wang, H. Liu, T. He, Y. Wang, S. Li and M. Yan, *J. Power Sources*, 2019, **438**, 227006–227016.
9 M. Y. Song and Y. J. Kwak, *Mater. Res. Bull.*, 2021, **140**, 111304.
10 X. Lin, S. Li, H. He, Z. Wu, J. Wu, L. Chen, D. Ye and M. Fu, *Appl. Catal., B*, 2018, **223**, 91–102.
11 P. Liu, H. Chen, H. Yu, X. Liu, R. Jiang, X. Li and S. Zhou, *Int. J. Hydrogen Energy*, 2019, **44**, 13606–13612.
12 J. Xiong, Y. C. Wei, Y. L. Zhang, X. L. Mei, Q. Q. Wu, Z. Zhao, J. Liu, D. Wu and J. M. Li, *Catal. Today*, 2020, **355**, 587–595.
13 J. Xiong, X. Mei, J. Liu, Y. Wei, Z. Zhao, Z. Xie and J. Li, *Appl. Catal., B*, 2019, **251**, 247–260.
14 S. Ali, L. Chen, F. Yuan, R. Li, T. Zhang, S. u. H. Bakhtiar, X. Leng, X. Niu and Y. Zhu, *Appl. Catal., B*, 2017, **210**, 223–234.
15 Y. Cheng, W. Song, J. Liu, H. Zheng, Z. Zhao, C. Xu, Y. Wei and E. J. M. Hensen, *ACS Catal.*, 2017, **7**, 3883–3892.
16 X. Zhang, K. Wang, X. Zhang, J. Hu, M. Gao, H. Pan and Y. Liu, *Int. J. Energy Res.*, 2021, **45**, 3129–3141.
17 N. A. Sazelee, N. H. Idris, M. F. Md Din, N. S. Mustafa, N. A. Ali, M. S. Yahya, F. A. Halim Yap, N. N. Sulaiman and M. Ismail, *Int. J. Hydrogen Energy*, 2018, **43**, 20853–20860.
18 L. Dan, L. Hu, H. Wang and M. Zhu, *Int. J. Hydrogen Energy*, 2019, **44**, 29249–29254.
19 S. Singh, A. Bhatnagar, V. Shukla, A. K. Vishwakarma, P. K. Soni, S. K. Verma, M. A. Shaz, A. S. K. Sinha and O. N. Srivastava, *Int. J. Hydrogen Energy*, 2020, **45**, 774–786.
20 N. A. Ali, N. H. Idris, M. F. M. Din, M. S. Yahya and M. Ismail, *J. Alloys Compd.*, 2019, **796**, 279–286.
21 D. Pukazhselvan, N. Nasani, P. Correia, E. Carbó-Argibay, G. Otero-Irurueta, D. G. Stroppa and D. P. Fagg, *J. Power Sources*, 2017, **362**, 174–183.
22 N. A. Sazelee, N. H. Idris, M. F. Md Din, M. S. Yahya, N. A. Ali and M. Ismail, *Results Phys.*, 2020, **16**, 102844.
23 L. T. Zhang, Z. L. Cai, X. Q. Zhu, Z. D. Yao, Z. Sun, L. Ji, N. H. Yan, B. B. Xiao and L. X. Chen, *J. Alloys Compd.*, 2019, **805**, 295–302.
24 J. S. Pedersen, *J. Appl. Crystallogr.*, 1994, **27**, 595–608.
25 N. S. Mustafa and M. Ismail, *J. Alloys Compd.*, 2017, **695**, 2532–2538.
26 Y. Cheng, J. Liu, Z. Zhao, W. Song and Y. Wei, *J. Hazard. Mater.*, 2018, **342**, 317–325.
27 Y. Cheng, J. Liu, Z. Zhao, W. Song and Y. Wei, *Chem. Eng. Sci.*, 2017, **167**, 219–228.
28 X. Yuan, H. Ge, X. Liu, X. Wang, W. Chen, W. Dong and F. Huang, *J. Alloys Compd.*, 2016, **688**, 613–618.
29 J. Fan, X. Wu, X. Wu, Q. Liang, R. Ran and D. Weng, *Appl. Catal., B*, 2008, **81**, 38–48.
30 Z. Cao, L. Ouyang, H. Wang, J. Liu, L. Sun and M. Zhu, *J. Alloys Compd.*, 2015, **639**, 452–457.
31 D. Wu, L. Ouyang, C. Wu, H. Wang, J. Liu, L. Sun and M. Zhu, *J. Alloys Compd.*, 2015, **642**, 180–184.
32 L. Z. Ouyang, X. S. Yang, M. Zhu, J. W. Liu, H. W. Dong, D. L. Sun, J. Zou and X. D. Yao, *J. Phys. Chem. C*, 2014, **118**, 7808–7820.
33 M. Ismail, N. S. Mustafa, N. A. Ali, N. A. Sazelee and M. S. Yahya, *Int. J. Hydrogen Energy*, 2019, **44**, 318–324.
34 N. A. Ali, N. H. Idris, M. F. M. Din, N. S. Mustafa, N. A. Sazelee, F. A. H. Yap, N. N. Sulaiman, M. S. Yahya and M. Ismail, *RSC Adv.*, 2018, **8**, 15667–15674.
35 J.-R. Ares-Fernández and K.-F. Aguey-Zinsou, *Catalysts*, 2012, **2**, 330–343.
36 L. S. Xie, J. S. Li, T. B. Zhang and L. Song, *Mater. Charact.*, 2017, **133**, 94–101.